

End station for nanoscale magnetic materials study: Combination of scanning tunneling microscopy and soft X-ray magnetic circular dichroism spectroscopy

Tetsuro Ueno, Masahiro Sawada, Yusuke Kishimizu, Akio Kimura, Hirofumi Namatame et al.

Citation: *Rev. Sci. Instrum.* **83**, 123903 (2012); doi: 10.1063/1.4770126

View online: <http://dx.doi.org/10.1063/1.4770126>

View Table of Contents: <http://rsi.aip.org/resource/1/RSINAK/v83/i12>

Published by the [American Institute of Physics](http://www.aip.org).

Related Articles

Intermetallic compound formation at Cu-Al wire bond interface
J. Appl. Phys. **112**, 123501 (2012)

Length-dependent mechanical properties of gold nanowires
J. Appl. Phys. **112**, 114314 (2012)

Chemical and structural investigations of the incorporation of metal manganese into ruthenium thin films for use as copper diffusion barrier layers
Appl. Phys. Lett. **101**, 231603 (2012)

Single-step holographic fabrication of large-area periodically corrugated metal films
J. Appl. Phys. **112**, 113101 (2012)

Role of Si in high Bs and low core-loss Fe_{85.2}B₁₀-XP₄Cu_{0.8}Si_x nano-crystalline alloys
J. Appl. Phys. **112**, 103902 (2012)

Additional information on Rev. Sci. Instrum.

Journal Homepage: <http://rsi.aip.org>


Journal Information: http://rsi.aip.org/about/about_the_journal

Top downloads: http://rsi.aip.org/features/most_downloaded

Information for Authors: <http://rsi.aip.org/authors>

ADVERTISEMENT

JANIS Does your research require low temperatures? Contact Janis today.
Our engineers will assist you in choosing the best system for your application.



10 mK to 800 K
Cryocoolers
Dilution Refrigerator Systems
Micro-manipulated Probe Stations

LHe/LN₂ Cryostats
Magnet Systems

sales@janis.com www.janis.com
Click to view our product web page.

End station for nanoscale magnetic materials study: Combination of scanning tunneling microscopy and soft X-ray magnetic circular dichroism spectroscopy

Tetsuro Ueno,¹ Masahiro Sawada,^{1,a)} Yusuke Kishimizu,² Akio Kimura,² Hirofumi Namatame,¹ and Masaki Taniguchi^{1,2}

¹Hiroshima Synchrotron Radiation Center, Hiroshima University, 2-313 Kagamiyama, Higashi-Hiroshima 739-0046, Japan

²Graduate School of Science, Hiroshima University, 1-3-1 Kagamiyama, Higashi-Hiroshima 739-8526, Japan

(Received 1 October 2012; accepted 21 November 2012; published online 19 December 2012)

We have constructed an end station for nanoscale magnetic materials study at the soft X-ray beamline HiSOR BL-14 at Hiroshima Synchrotron Radiation Center. An ultrahigh-vacuum scanning tunneling microscope (STM) was installed for an *in situ* characterization of nanoscale magnetic materials in combination with soft X-ray magnetic circular dichroism (XMCD) spectroscopy experiment. The STM was connected to the XMCD experimental station via damper bellows to isolate it from environmental vibrations, thus achieving efficient spatial resolution for observing Si(111) surface at atomic resolution. We performed an *in situ* experiment with STM and XMCD spectroscopy on Co nanoclusters on an Au(111) surface and explored its practical application to investigate magnetic properties for well-characterized nanoscale magnetic materials. © 2012 American Institute of Physics. [<http://dx.doi.org/10.1063/1.4770126>]

I. INTRODUCTION

Nanotechnology, based on material surfaces and nanoscale materials, has become increasingly important to the sustainable development of today's human society. Characteristic physical and chemical properties are used for industrial applications such as semiconductor devices, catalysts, fuel cells, sensors, optical materials, magnetic materials, and so on. In particular, magnetic properties of nanoscale magnetic materials such as perpendicular magnetic anisotropy¹ and giant magnetoresistance^{2,3} are currently used for high-density magnetic storage devices and will be extended to spintronics. These useful and remarkable properties come from characteristic electronic and atomic structures of nanoscale magnetic materials such as films, nanowires, nanodots, and surface magnetic molecules. For example, cobalt (Co) nanodots, each of which only consists of several Co atoms, on a platinum (Pt) surface exhibit an extraordinary giant orbital magnetic moment and magnetic anisotropy energy (MAE).⁴ Reduced number of coordinations of magnetic atoms at the surface result in unquenched orbital magnetic moments and giant MAEs. It is believed that the atomic structures of nanoscale magnetic materials strongly correlate with the magnetic properties. Therefore, it is essential to determine the atomic structures and magnetic properties of a sample at the same time, if possible.

Atomic structures of surface nanoscale materials are directly observed by means of a scanning probe microscope (SPM) equipped with an atomic-scale apex probe. By scanning a probe on the surface and detecting electric charge, atomic force or other forces as a function of two-dimensional

positions, an SPM is able to visualize surface structures on the atomic scale. The scanning tunneling microscope (STM)⁵ is a prototype variation of the SPM that measures tunneling current between the surface and a probe. So far, STMs have been used to investigate the morphology and atomic structures of various nanoscale magnetic materials.^{6–10} In addition, spin-polarized STM¹¹ has found novel magnetic orders such as the surface skyrmion.¹²

However, an experimental method that directly observes electronic structure is needed to characterize the physical or chemical properties of nanoscale materials microscopically. X-ray absorption spectroscopy (XAS) is a spectroscopic method with synchrotron radiation that probes unoccupied electronic states of materials. Magnetic signals can also be detected by XAS with X-ray magnetic circular dichroism (XMCD) by using circularly-polarized photons.¹³ Quantitative values of spin and orbital magnetic moments are determined separately from the XMCD spectrum using the magneto-optical sum rules.^{14,15} It is highly suitable for nanoscale materials because of its element specificity. This method has so far been applied to various surface nanoscale magnetic materials such as nanoclusters,¹⁶ nanowires,^{17,18} nanodots,⁴ isolated atoms,¹⁹ and magnetic molecules.²⁰

Thus, combining STM and XMCD spectroscopy is an effective way to reveal the microscopic origins of the magnetic properties of well-characterized nanoscale magnetic materials. However, up to now, STM and XMCD spectroscopy are generally individual experimental techniques used in separate apparatuses, except for very few examples such as synchrotron-radiation-excited STM.^{21–23,25} Scanning tunneling microscopy is very vibration-sensitive because it requires a probe-sample distance on the nanometer order and high precision of the lateral position of a probe. A synchrotron facility is full of environmental vibrations from the mechanical

^{a)} Author to whom correspondence should be addressed. Electronic mail: sawa@hiroshima-u.ac.jp.

pumps, refrigerators, or motion of users working at the beamline. Thus, STM and synchrotron facilities are incompatible, and very few synchrotron facilities have beamlines with STM.^{20,22–25} To perform an *in situ* STM or XMCD experiment, all vacuum-chambers are interconnected with each other, and samples can be transferred from one to the other without breaking an ultrahigh-vacuum (UHV) condition. The STM system and a beamline must be connected rigidly to satisfy this requirement. However, the rigid connection impairs the performance of the vibration-isolation table of STM and makes it difficult to attain sufficient spatial resolution. Therefore, two conflicting conditions (rigid UHV connection and vibration isolation) must be overcome to combine STM and XMCD spectroscopy.

We have been constructing the end station for researching nanoscale magnetic materials at the soft X-ray beamline HiSOR BL-14 at Hiroshima Synchrotron Radiation Center (HSRC).²⁶ In this paper, we report the beamline connection of a ready-made UHV-STM system at HiSOR BL-14 and demonstrate its potential to study nanoscale magnetic materials in combination with soft X-ray spectroscopy experiment. It will be shown that damper bellows (bellows with support rods and rubber dampers) sufficiently isolate the STM system from environmental vibrations for practical use. As a result, we have successfully realized the suppressed vibration circumstance for general purpose via the newly installed intermediate chamber.

II. EXPERIMENTAL SYSTEM

HiSOR BL-14 at HSRC equips an inverse-dragon type monochromator at the bending-magnet source of the electron storage ring. It is designed for experiments using polarized soft X-rays such as XMCD or X-ray linear dichroism spectroscopy.²⁷ The photon energy range of this beamline ($h\nu = 100\text{--}1200$ eV) is suitable for XAS experiments at the *K* edge of light elements, *L* edges of *3d* transition metals, and *M* edges of *4d* transition metals. Lateral and vertical beam size at the sample position are 3 mm and 0.5 mm, respectively. Photon flux is approximately 10^{10} photons/s in the photon energy range from 700 to 800 eV. Figure 1 shows the schematic of the end stations of HiSOR BL-14. An XMCD measurement apparatus is installed at the first focal point in the beamline, which is composed of a UHV chamber with a permanent magnet array ($B = 1.3$ T), an electromagnet ($B = 0.3$ T maximum) for XMCD experiments and a sample manipulator with a liquid N_2 cryostat. A sample preparation chamber is connected to the XMCD chamber in UHV. The sample preparation chamber is equipped with instruments for thin-film fabrication and characterization. Details of this system are given in the literature.²⁶

We have newly constructed an intermediate chamber for interconnecting the existing XMCD experimental system and a stand-alone UHV-STM system. The intermediate chamber guarantees vibration-isolation docking of the STM system and a sample transfer path to the XMCD chamber under UHV. Details of the intermediate chamber will be given in Sec. III.

The UHV-STM system (UHV 300, RHK Technology) has an independent sample preparation chamber that is di-

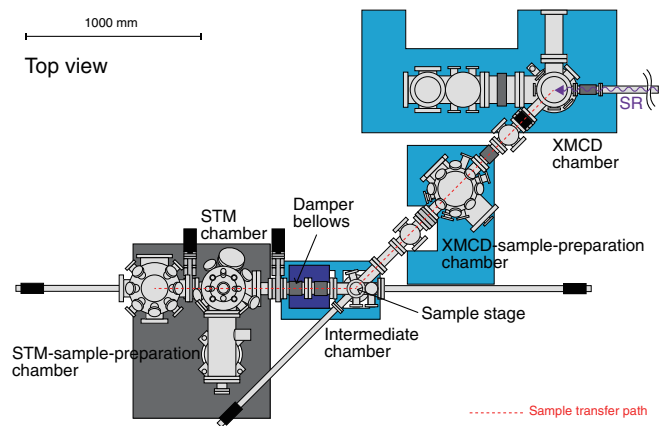


FIG. 1. Schematic of the end station of HiSOR BL-14. The red dashed line represents the sample transfer path from the STM-sample-preparation chamber to the XMCD chamber. The purple wavy arrowed line represents the photon incident direction to the XMCD chamber.

rectly connected to the STM chamber. The STM-sample-preparation chamber is equipped with sample fabrication and characterization instruments. We used this chamber to prepare the sample for the *in situ* STM and XMCD experiment described in Sec. IV. A clean surface of an Au(111) single crystalline substrate was prepared with repeated cycles of Ar^+ bombardment and annealing to 970 K. Negligible contamination was found in Auger electron spectra. Co was deposited onto the substrate at room temperature by using an electron beam evaporator.

III. CONNECTION OF STM APPARATUS AT BEAMLINE

A. Isolation of STM from environmental vibrations

Because the STM is extremely vibration-sensitive, it is necessary to isolate the STM system from the vibrations generated from various sources in the synchrotron facility. The STM chamber is mounted on a heavy stone table to remove vibration via air suspension. An eddy current damper is also installed inside the STM chamber to isolate finely the vibration propagated to the measurement stage. The characteristic frequencies of the heavy stone table and the eddy current damper are about 10 Hz and 1.5 Hz, respectively. Thus, the STM system works well in a stand-alone operation with the duplex configuration of the vibration-isolation system, which cuts off higher-frequency vibration components from the building floor.

The intermediate chamber is rigidly interconnected with the XMCD-sample-preparation chamber in UHV. To avoid generating mechanical vibrations, the intermediate chamber is only equipped with an ion pump (PST-100CX, ULVAC) to keep UHV. A scroll pump and a turbo molecular pump are used only in rough pumping during bakeout and disconnected after running the ion pump. As mentioned above, it is necessary to connect all the chambers rigidly under UHV. However, the rigid connection makes the intermediate chamber the propagating path of vibrations from the XMCD experimental system. These contradicting situations seem to be settled by using simple bellows, because the bellows can prevent

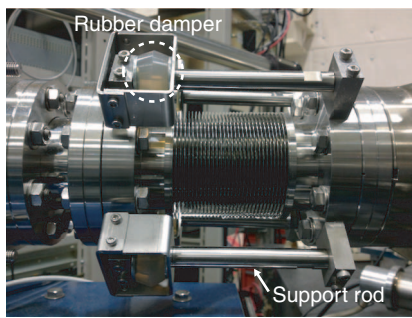


FIG. 2. Damper bellows connected between the STM chamber and the intermediate chamber.

vibrations propagating to the STM system. However, contractile forces shorten the length of bellows under UHV. As a consequence, the heavy stone table with air suspension is fixed because of the lateral shift via shorten bellows and the functionality of the vibration isolation is compromised.

Thus, bellows with support rods are necessary to avoid contraction of bellows, though the support rods become the propagating path of vibrations. Therefore, we introduced damper bellows to a docking port of the intermediate chamber as shown in Fig. 2. Four support rods connected with rubber dampers prevent the bellows from contracting under UHV. Four rubber dampers damp down and cut off vibrations propagating through the intermediate chamber. The lateral position of the STM system is adjusted to the balanced position under UHV so as not to lock the air suspension table. Thus,

we achieve a vibration-isolation rigid connection of the STM system under UHV. The docking port is also equipped with an XY stage for fine adjustment of the docking positions. The STM chamber is connected to the docking port. However, this port is not only for the current STM system, but also works as a utility port for other stand-alone experimental apparatuses that require a vibration-isolation environment.

To confirm the vibration-isolation connection of the STM system, we measured the STM topography of the Si(111) surface with a tungsten tip as a standard sample for the UHV-STM system before and after the beamline connection. Figures 3(a) and 3(b) show STM topographic images of Si(111) before (offline) and after (online) connection of the STM chamber to the intermediate chamber. Both images clearly show the 7×7 reconstructed surface of Si(111) at atomic resolution. Height profiles along the white lines in Figs. 3(a) and 3(b) are shown in Figs. 3(c) and 3(d), respectively. These profiles are qualitatively identical before and after the beamline connection except for the contrast, which is better in the offline experiment. The decrease in contrast is attributable to inevitable vibrations by the beamline connection. Two STM images were taken with use of tungsten tips with the similar radius of curvature prepared by same etching treatment. However, the difference in contrast may be attributable to the minor change in tip conditions such as adsorbate on the tip. The width of each peak in the height profiles is about 2.8 \AA and 3.5 \AA for the offline and online experiments, respectively. Thus, the lateral spatial resolution becomes worse with the beamline connection. Vertical spatial resolution after the

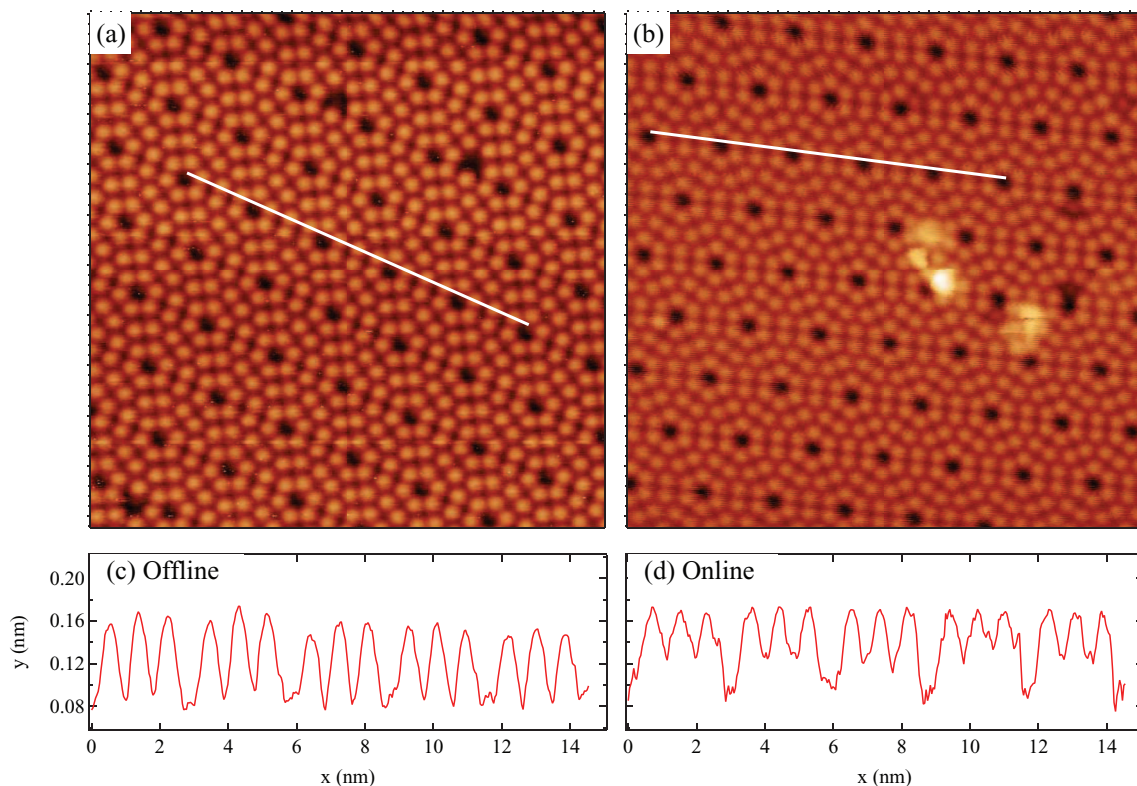


FIG. 3. STM topographic images of Si(111) 7×7 surface (a) before and (b) after connection to the intermediate chamber. The tip bias was set to 2.0 V, and the tunneling current was set to 0.15 nA. The lateral size is $20 \times 20 \text{ nm}^2$. Height profiles along the white lines in (a) and (b) are shown in (c) and (d), respectively.

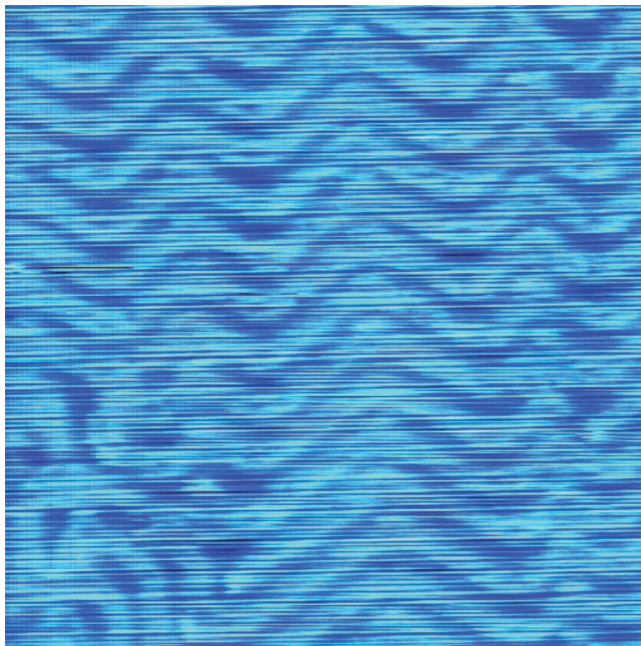


FIG. 4. STM topographic images of Au(111)- $\sqrt{3} \times 23$ herringbone reconstruction. The tip bias was set to 0.5 V, and the tunneling current was set to 0.15 nA. The lateral size is 100×100 nm².

beamline connection was evaluated as 0.08 Å from the height profile in Fig. 3(d). We conclude that the effect of vibrations from the beamline connection is maximally suppressed, and there is no problem with taking topographic images of Si surfaces at atomic resolution.

We also obtained an STM image of the Au(111) surface. Au(111) exhibits surface reconstruction with $\sqrt{3} \times 23$ periodicity, which is called herringbone reconstruction.²⁸ We clearly observed the herringbone reconstruction of the Au(111) surface with the UHV-STM system even after the beamline connection (Fig. 4). This indicates that the UHV-STM system at HiSOR BL-14 achieves sufficient vertical spatial resolution to characterize the metal surface with an asperity of 0.2 Å.²⁸ Substantially noisier image of Au(111) than that of Si(111) [see Figs. 3(a) and 3(b)] comes from the signal-to-noise ratio in the measurement. Because the localized electrons in the semiconductor Si surface are advantageous to get better contrast than the delocalized electrons in the metallic Au surface even in the similar experimental conditions.

B. Sample transfer

Because the existing XMCD experimental system and the ready-made stand-alone UHV-STM system are interconnected with each other, the sample transfer system needs to be attached. Figure 5 shows schematics of the sample plate and sample holders for STM and XMCD. The sample plate is a 1-mm-thick Mo plate for mounting the sample directly. The STM holder is a modified version of a commercial STM holder with a ramp for a beetle-type STM scan head.²⁹ Side loading of the sample plate is possible while keeping the dimensions of the original one. The XMCD holder is designed

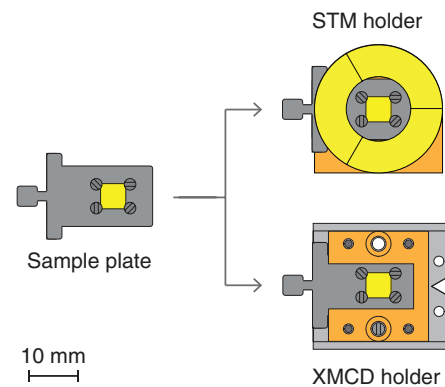


FIG. 5. Schematics of sample plate and sample holders for STM and XMCD experiments. The yellow square represents the sample, which has a size of 5×5 mm².

to fit a sample manipulator of the existing XMCD system. The total thickness of the XMCD holder must be below 5 mm, because the permanent magnet in the XMCD chamber has a gap of only 10 mm to insert the sample. The sample plate can be nested in both the STM holder and the XMCD holder for each experiment as shown in Fig. 5.

The intermediate chamber is equipped with two transfer rods, one to transfer to the STM chamber and another to transfer to the XMCD-sample-preparation chamber as shown in Fig. 1. It is also equipped with a four-axis (X, Y, Z, and θ) sample stage. The STM holder is put on the sample stage and rotated to pick up the sample plate with each transfer rod. Figure 1 shows the sample transfer path from the STM-sample-preparation chamber to the XMCD chamber. The amount of time required to transfer the sample from the STM chamber to the measurement position of the XMCD chamber is about 30 min. The base pressure of each chamber is shown in Table I. Surface contamination of the sample can be minimized by passing the intermediate chamber for a short time.

IV. *IN SITU* STM AND XMCD EXPERIMENT

To examine the performance of the whole system, we carried out an *in situ* STM and XMCD experiment on nanostructured Co on an Au(111) surface. It is known that two-monolayer-height Co clusters grow by self-assembly on the elbow site of the herringbone reconstruction of an Au(111) surface.⁶ In addition, Co nanoclusters on Au(111) exhibit an easy magnetization axis perpendicular to the surface.³⁰

TABLE I. Base pressure of each chamber of the end station of HiSOR BL-14.

Chamber	Pressure (Pa)
STM-sample-preparation	3×10^{-8}
STM	2×10^{-9}
Intermediate	6×10^{-7}
XMCD-sample-preparation	5×10^{-8}
XMCD	4×10^{-8}

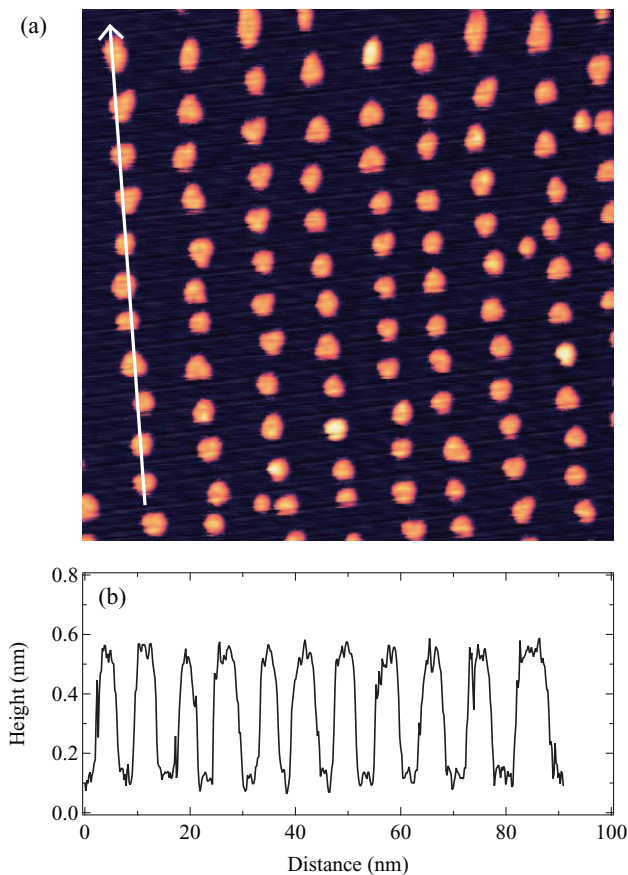


FIG. 6. (a) STM topographic image of Co clusters on Au(111) surface. The tip bias was set to 2.0 V, and the tunneling current was set to 0.15 nA. The lateral size is $100 \times 100 \text{ nm}^2$. (b) Line profile along the arrow in (a).

Figure 6(a) shows an STM topographic image of Co clusters on Au(111). Periodically distributed Co clusters are observed. The line profile along an arrow in Fig. 6(a) is shown in Fig. 6(b). The cluster height is about 4 Å, which is comparable to the lattice constant of hcp Co ($c = 4.07 \text{ Å}$). This indicates the height of Co clusters as 2 monolayers (ML).

Figure 7(a) shows an STM topographic image of another set of deposition for Co on Au(111) with the larger Co coverage than that in Fig. 6(a). The bright area denotes Co clusters with a larger lateral size than in Fig. 6(a). In Fig. 7(b), three remarkable peaks appear in the height distribution of the STM topographic image in Fig. 7(a). These peaks around 0.2, 0.6, and 0.8 nm correspond to the frequencies of Au substrate, 2 ML Co, and 3 ML Co, respectively. Thus, we directly found the coexistence of 2 ML and 3 ML Co clusters in increased Co coverage. This kind of microscopic morphological information is difficult to obtain from the on-site analysis of reciprocal space observation such as low-energy electron diffraction. The STM system at HiSOR-BL14 has the capability to measure nanoclusters with a diameter of only a few nm and height of only a few monolayers. *In situ* magnetic measurement of these nanoclusters enables us to understand in detail the correlation of the morphology with magnetism.

After the STM measurement, we transferred the sample to the XMCD chamber and performed a temperature-dependent XMCD experiment. The XMCD signal was ob-

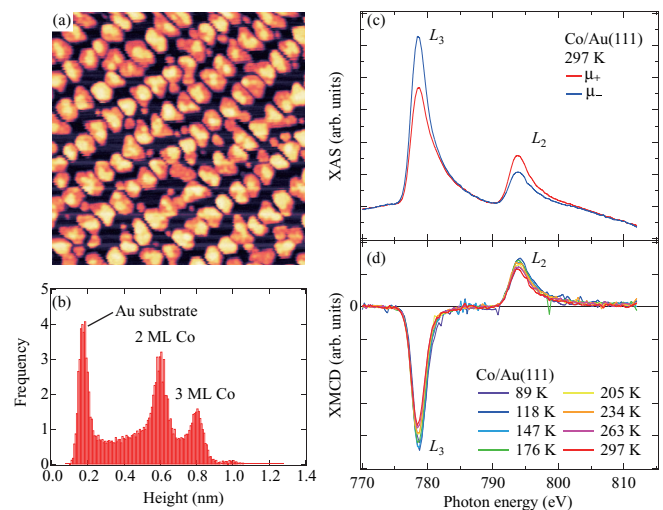


FIG. 7. (a) STM topographic image of Co/Au(111) ($100 \times 100 \text{ nm}^2$). (b) Height distribution in (a). (c) Co $L_{2,3}$ XAS at 297 K. Red (μ_+) and blue (μ_-) curves represent XAS for different magnetization direction. (d) Temperature dependence of Co $L_{2,3}$ XMCD spectra of Co/Au(111). All XMCD spectra are normalized by the L_3 intensity of XAS spectra. These data are collected *in situ* for the same sample.

tained with a perpendicular magnetic field of 1.3 T using the permanent magnet. Photon incident angle was set normal to the surface. Beam spot size at the sample surface is much larger than the area scanned in the STM measurement. Therefore, the uniformness of the sample surface must be guaranteed. We have checked the homogeneity of the sample surface by the Auger electron spectra at multiple measurement points. Figure 7(c) shows X-ray absorption spectra of Co/Au(111) at Co $L_{2,3}$ edges at room temperature (297 K). We clearly observe an intensity difference at two white lines (L_3 and L_2) with magnetization direction. To investigate the magnetic behavior of Co nanoclusters, we measured the temperature dependence of Co $L_{2,3}$ XMCD spectra [see Fig. 7(d)]. We first cooled the sample to 89 K by flowing liquid N_2 under the magnetic field and then the data were acquired with increasing temperature. The amplitude of the XMCD spectra, which corresponds to the magnetization, gradually increases with decreasing temperature and almost saturates below 176 K within measurement precision. This indicates that our XMCD experimental system with a liquid N_2 cryostat can detect the magnetic signal of ferromagnetic nanoclusters with a diameter of a few nm and height of a few monolayers. A higher magnetic field and lower temperature are desirable in order to perform XMCD experiments for smaller magnets such as nanodots or magnetic molecules.

As shown above, we have successfully demonstrated an *in situ* STM and XMCD experiment on nanoscale magnetic materials. It is possible to use an *in situ* STM and XMCD experiment to measure a cluster-size- and/or cluster-height-dependent magnetization. STM can directly observe surface morphology and obtain statistics such as cluster-size and cluster-height distribution. Thus, it is possible to deduce cluster-size- and/or cluster-height-dependent XMCD spectra through a simultaneous analysis of several data sets of STM topography and the corresponding XMCD spectra.

V. SUMMARY

We have developed an end station for nanoscale magnetic materials study at the soft X-ray beamline HiSOR BL-14 at HSRC. The stand-alone UHV-STM system is connected to the end station of the beamline via damper bellows. It achieves sufficient spatial resolution to observe surface nanoscale magnetic materials. We have demonstrated an *in situ* STM and XMCD combination experiment on Co nanoclusters on Au(111) and emphasized the importance of real-space observation of morphology with magnetization measurement. These results would provide useful information on the other potential end stations of the synchrotron facilities in the world, where the SPM is already or planned to be installed. As demonstrated in this report, the combination of SPM with the synchrotron radiation experiments will accelerate the materials research especially in nano-science field.

ACKNOWLEDGMENTS

All the experiments were performed at the HSRC under the approval of the Proposal Assessing Committee. This work was in part supported by Research Fellowships of the Japan Society for the Promotion of Science for Young Scientists (No. 21 · 2032). The authors would like to thank Dr. Mao Ye, Dr. Yitao Cui, and Dr. Osamu Morimoto for technical assistance with the STM experiments. We are grateful to Dr. Koji Miyamoto for helpful comments on the manuscript. All STM images were analyzed with Gwyddion (Gwyddion 2.25, GNU General Public License, <http://www.gwyddion.net>, 2011).

¹W. B. Zeper, F. J. A. M. Greidanus, P. F. Carcia, and C. R. Fincher, *J. Appl. Phys.* **65**, 4971 (1989).

²M. N. Baibich, J. M. Broto, A. Fert, F. Nguyen Van Dau, F. Petroff, P. Etienne, G. Creuzet, A. Friederich, and J. Chazelas, *Phys. Rev. Lett.* **61**, 2472 (1988).

³G. Binasch, P. Grünberg, F. Saurenbach, and W. Zinn, *Phys. Rev. B* **39**, 4828 (1989).

⁴P. Gambardella, S. Rusponi, M. Veronese, S. S. Dhesi, C. Grazioli, A. Dallmeyer, I. Cabria, R. Zeller, P. H. Deverichs, K. Kern, C. Carbone, and H. Brune, *Science* **300**, 1130 (2003).

⁵G. Binnig, H. Rohrer, Ch. Gerber, and E. Weibel, *Phys. Rev. Lett.* **49**, 57 (1982).

⁶B. Voigtländer, G. Meyer, and N. M. Amer, *Phys. Rev. B* **44**, 10354 (1991).

⁷J. de la Figuera, J. E. Prieto, C. Ocal, and R. Miranda, *Phys. Rev. B* **47**, 13043 (1993).

⁸J. Shen, J. Giergiel, and J. Kirschner, *Phys. Rev. B* **52**, 8454 (1995).

⁹S. M. Jordan, R. Schad, A. M. Keen, M. Bischoff, D. S. Schmool, and H. van Kempen, *Phys. Rev. B* **59**, 7350 (1999).

¹⁰M. Pratzner and H. J. Elmers, *Phys. Rev. Lett.* **90**, 077201 (2003).

¹¹R. Wiesendanger, *Rev. Mod. Phys.* **81**, 1495 (2009).

¹²S. Heinze, K. von Bergmann, M. Menzel, J. Brede, A. Kubetzka, R. Wiesendanger, G. Bihlmayer, and S. Blügel, *Nat. Phys.* **7**, 713 (2011).

¹³C. T. Chen, F. Sette, Y. Ma, and S. Modesti, *Phys. Rev. B* **42**, 7262 (1990).

¹⁴B. T. Thole, P. Carra, F. Sette, and G. van der Laan, *Phys. Rev. Lett.* **68**, 1943 (1992).

¹⁵P. Carra, B. T. Thole, M. Altarelli, and X. Wang, *Phys. Rev. Lett.* **70**, 694 (1993).

¹⁶T. Koide, H. Miyauchi, J. Okamoto, T. Shidara, A. Fujimori, H. Fukutani, K. Amemiya, H. Takeshita, S. Yuasa, T. Katayama, and Y. Suzuki, *Phys. Rev. Lett.* **87**, 257201 (2001).

¹⁷P. Gambardella, A. Dallmeyer, K. Maiti, M. C. Malagoli, W. Eberhardt, K. Kern, and C. Carbone, *Nature (London)* **416**, 301 (2002).

¹⁸H. Fujisawa, S. Shiraki, M. Furukawa, S. Ito, T. Nakamura, T. Muro, M. Nantoh, and M. Kawai, *Phys. Rev. B* **75**, 245423 (2007).

¹⁹H. Brune and P. Gambardella, *Surf. Sci.* **603**, 1812 (2009).

²⁰P. Gambardella, S. Stepanow, A. Dmitriev, J. Honolka, F. M. F. de Groot, M. Lingenfelder, S. S. Gupta, D. D. Sarma, P. Bencok, S. Stanesco, S. Clair, S. Pons, N. Lin, A. P. Seitsonen, H. Brune, J. V. Barth, and K. Kern, *Nature Mater.* **8**, 189 (2009).

²¹V. Rose, T. Y. Chien, J. W. Freeland, D. Rosenmann, J. Hiller, and V. Metlushko, *J. Appl. Phys.* **111**, 07E304 (2012).

²²T. Matsushima, T. Okuda, T. Eguchi, M. Ono, A. Harasawa, T. Wakita, A. Kataoka, M. Hamada, A. Kamoshida, Y. Hasegawa, and T. Kinoshita, *Rev. Sci. Instrum.* **75**, 2149 (2004).

²³A. Saito, J. Maruyama, K. Manabe, K. Kitamoto, K. Takahashi, K. Takami, M. Yabashi, Y. Tanaka, D. Miwa, M. Ishii, Y. Takagi, M. Akai-Kasaya, S. Shin, T. Ishikawa, Y. Kuwahara, and M. Aono, *J. Synchrotron Radiat.* **13**, 216 (2006).

²⁴G. Panaccione, I. Vobornik, J. Fujii, D. Krizmancic, E. Annese, L. Giovannelli, F. Maccherozzi, F. Salvador, A. De Luisa, D. Benedetti, A. Gruden, P. Bertoch, F. Polack, D. Cocco, G. Sostero, B. Diviacco, M. Hochstrasser, U. Maier, D. Pesca, C. H. Back, T. Greber, J. Osterwalder, M. Galaktionov, M. Sancrotti, and G. Rossi, *Rev. Sci. Instrum.* **80**, 043105 (2009).

²⁵M. L. Cummings, T. Y. Chien, C. Preissner, V. Madhavan, D. Diesing, M. Bode, J. W. Freeland, and V. Rose, *Ultramicroscopy* **112**, 22 (2012).

²⁶M. Sawada, T. Ueno, T. Tagashira, H. Namatame, and M. Taniguchi, *AIP Conf. Proc.* **1234**, 939 (2010).

²⁷M. Sawada, K. Yaji, M. Nagira, A. Kimura, H. Namatame, and M. Taniguchi, *AIP Conf. Proc.* **879**, 551 (2007).

²⁸J. V. Barth, H. Brune, G. Ertl, and R. J. Behm, *Phys. Rev. B* **42**, 9307 (1990).

²⁹R. R. Schulz and C. Rossel, *Rev. Sci. Instrum.* **65**, 1918 (1994).

³⁰S. Padovani, I. Chado, F. Scheurer, and J. P. Bucher, *Phys. Rev. B* **59**, 11887 (1999).